Journal of Visualization, Vol. 4, No. 3 (2001) 245-256

Integrated Approach to Computational and Experimental Flow Visualization of a Double Annular Confined Jet

Vucinic, D.* and Hazarika, B. K.*

* Department of Fluid Mechanics (STRO), Vrije Universiteit Brussel (VUB), Pleinlaan 2, B-1050 Brussels, Belgium.
e-mail: dean@stro.vub.ac.be

Received 12 March 2001.
Revised 2 July 2001.

***Abstract*:** The cold flow of a prototype industrial burner in a cylindrical combustion chamber is investigated. Two concentric annular axial jets simulate this complex flow field, which is investigated using Laser Sheet flow Visualization (LSV), Digital Particle Image Velocimetry (DPIV), Laser Doppler Velocimetry (LDV) and Computational Fluid Dynamics (CFD). The aim is to advance the physical understanding of combustion chamber flow fields and to assist the development of CFD codes specialized in such flows. These simulations generate large amount of data for various measured and calculated quantities. Thus, visualization and comparison procedures are applied for the validation of obtained results. The study reported here is one of the experiments applied in the design of the Quantitative Flow Field Visualization (QFView) software, a web-based environment which supports distributed data access. The application of QFView data analysis greatly improved the understandings about the various transition regions of the flow under investigation.

***Keywords*:** burner, annular jet, quantitative visualization, LSV, LDV, DPIV, CFD, database.

1. Introduction

Mixing of jets, often in enclosed space, plays a crucial role in a large number of industrial appliances. Unfortunately, the CFD codes are unable to predict complex turbulent flow fields accurately. During the development of these appliances a substantial part of the expenditures are necessary for experimental fluid dynamics (EFD). Thus, the EFD costs can be considerably reduced by development of reliable solvers to predict these flows. A two-stage validation of the CFD code is necessary to predict the process in the combustion chamber. First stage involves the prediction of the flow without chemical reactions followed by the second stage where chemical reactions are present.

The most significant fluid dynamic parameter involved in the combustion process of a jet is the Non-isothermal Craya-Curtet number (NCCN) as demonstrated by Guruz et al. (1974) and Steward and Guruz (1977). Care should also be taken to maintain geometrical similarity and the Reynolds number. Usually, it is not possible to establish the values of all similarity parameters equal between the experimental and prototype conditions. Thus their influence on the flow field should be assessed accurately.

Recently, the main thrust in design of the new burners has been to reduce the production of NO_x during combustion. The production of thermal NO_x is influenced by the flame temperature and oxygen concentration in the combustion zone. Therefore, a large stable flame front with uniform temperature leads to a substantially

reduced production of NO_x. The present burner was designed to supply the air through two concentric annular nozzles. The natural gas is injected in the central portion of the burner through a grid of small holes or through another concentric annular nozzle. This creates two regions of bluff body flame holders.

Due to the constraints on space, the designed burner admits air perpendicular to the burner axis through two circular tubes. The two streams of air enter the two concentric annular ducts leading to the nozzles. The contraction ratio slightly greater than 2 is used between the duct and the nozzles. The 90-degree flow turning and short annular duct, makes the exit flow field severely distorted from axisymmetry. Characterizing such a flow field is nearly impossible, making the task of CFD code validation extremely difficult. It is intended to circumvent this difficulty by conducting the physical and the numerical experiments in two phases. For a model of the prototype and the prototype itself, the flow was investigated at 4 meridional planes 45-degrees apart. These form the validation data for the industrial burner, which is not axisymmetric. For code development and calibration, the physical model needs to deliver an axisymmetric flow field where high-resolution data for the stationary flow field could be acquired. During the course of this investigation the study of instantaneous flow fields and effects of large coherent structures on the development of the flow field was found to be essential.

2. Integrated Approach with Quantitative Flow Field Visualization (QFView)

The rapid progress in all facets of fluid dynamics research has made it essential that the research activities are conducted in close cooperation between experimentalists, numerical analysts and theoreticians. In the early stages of the CFD development the improvements of the process was so rapid that it was expected to eliminate the role of EFD all together. However, experience showed that in order to study new phenomena experiments are still the most economical approach. The CFD codes, once validated against experimental data, are the most effective tool for the production of data to build a comprehensive flow database (Gharib, 1996).

The strengths of various tools in EFD and CFD should be used judiciously to extract significant quantities required for problem solving as shown in Fig. 1. In many cases it is essential to save all the data, instead of only the reduced data as it was done in the past. This eliminates the possibility of loss of information that was not considered important at the time the experiment was conducted, but later it was found to affect the results significantly. Both EFD and CFD used in Fig. 1, generate huge quantities of data, which could populate the database. The user needs to access, extract, visualize and compare the required quantities; these functions are illustrated in Fig. 2.

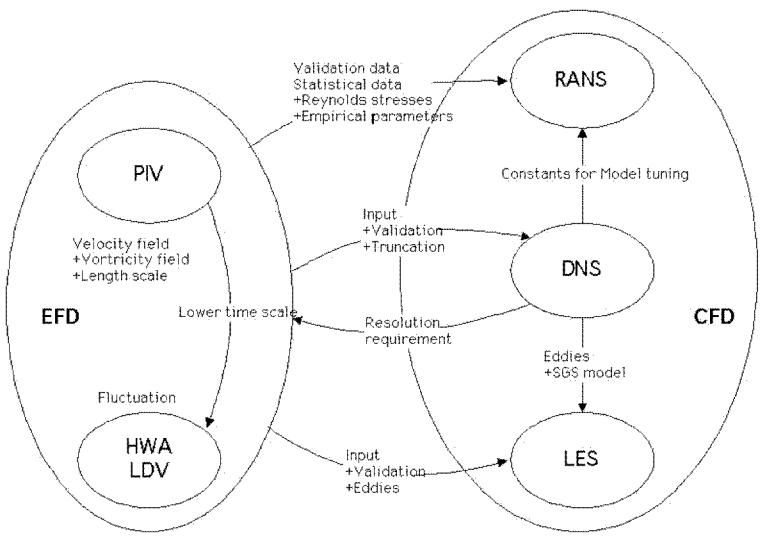

Fig. 1. Use of EFD and CFD tools.

The QFView software, used in this study, was designed to be open, web-based and component-based. It supports integrated application of the visualization and animation tools described in Vucinic et al. (1992, 2000, 2001) with focus on the application of database management system for data access and archiving. For example, a

possible distribution of the QFView components over the Internet can imply that the Enterprise JavaBeans (EJB, 2001), (JSP, 2000) and Relational Database Management System servers (RDBMS, 2001) are located in one place; while the GUI client applications are located at other geographically separated locations as shown in Fig. 3 (a).

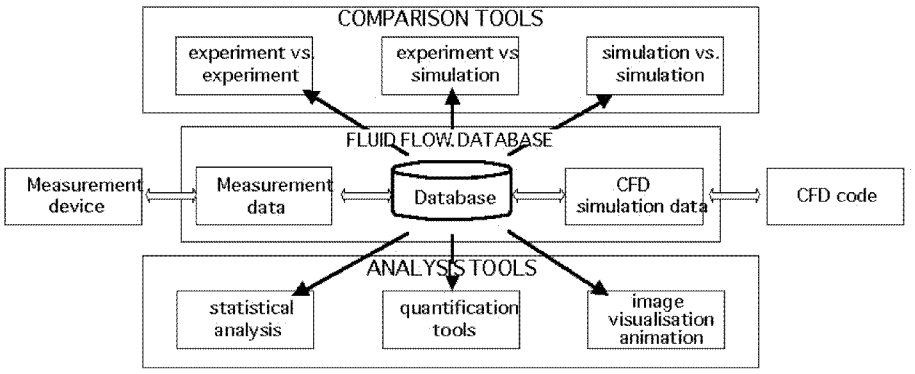

Fig. 2. The QFView framework.

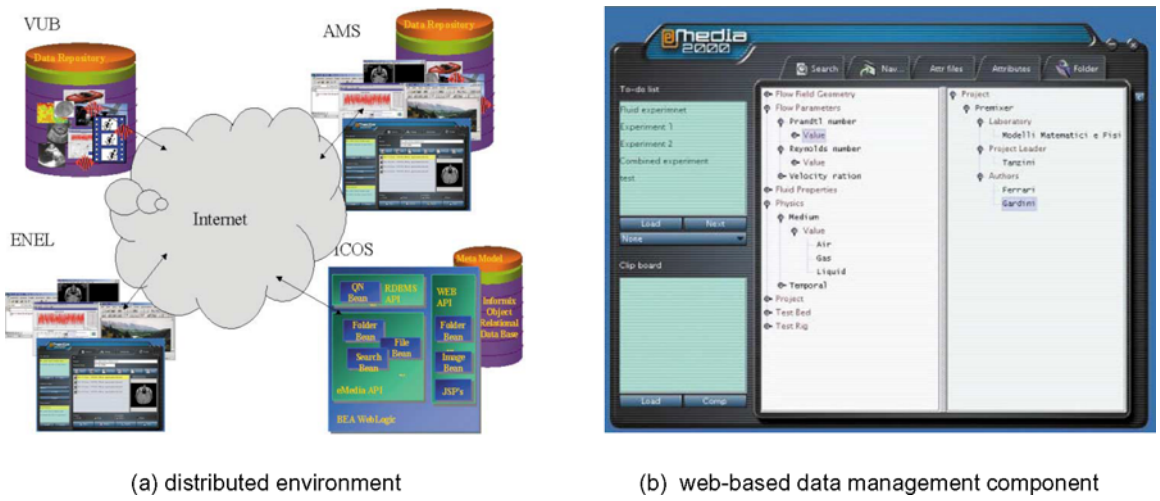

(a) distributed environment (b) web-based data management component

Fig. 3. QFView - an Internet based archiving and visualization environment.

The meta-database is based on J2EE, (J2EE, 2001), distributed architecture with execution logic stored and executed at the BEA WebLogic EJB container (BEA WebLogic, 2001) and accessed from the graphical user interface (GUI) based Java application via the HTTP protocol. The main advantage of the Internet is the possibility to store and access raw data (images, input files, text documents, etc.) from any URL globally accessed location. The QFView system is composed of three major elements listed below.

(1) WebLogic EJB container with all the metadata management rules to manipulate metadata and the Informix relational database used to store the metadata information. The EJB container acts as the security proxy for the data in the relational database.

(2) Thin GUI Java client is used for remote data entry, data organization and plug-in visualization. GUI clients must be installed at the end-user location, either by the application installation or the automatic application download (Zero Administration Client from WebLogic).

(3) URL accessed data (images, video, data files, etc.) can be placed at any URL site.

The QFView system organizes, stores, retrieves and classifies the data coming from experiments and simulations with an easy-to-use GUI. The data management component, see Fig. 3(b), offers a user-friendly web-enabled front-end to populate and maintain the metadata repository. The user can accomplish the following tasks using this thin GUI Java client:

- Start the GUI Java client application, create a new folder (measurement), define metadata information for the folder, such as keywords, physical characteristics, etc. It is important to emphasize that the GUI Java client is

connected to the EJB server using the HTTP protocol, and all the information entered by the user, as well as all changed information are automatically stored in the relational database.

- Organize the data into the hierarchy of predefined, or newly created tree like node; user can also execute a data search procedure, combine documents and do several other operations for the input folder.
- Create and define new raw data such as XML files, images, input files, etc. for the particular folder by specifying either a local or a remote location of the data.
- Define old raw data (XML files, text files, videos, etc.) by specifying either a local or a remote location of the data.
- Start the visualization plug-in application on the selected raw data.

Essential Database Tools present in QFView are:

a) Data Entry
b) Folder and Document Insertion
c) Data Classification
d) Full Text Search
e) Meta Model and Data Organization

These tools are used to assist the experiments setup, to improve the data acquisition and systematic manipulation of the obtained results.

3. Descriptions of Experiments

The prototype burner was designed to deliver 100 kW using natural gas. Several sets of preliminary combustion runs with a similar burner in the combustion chamber provided data for the realistic estimation of the non-dimensional parameters involved in the process. It was found that the parameters of the flow during operation will be maintained if the Reynolds number (Re_D), based on the primary jet diameter and the average velocity at the exit of the nozzle was 3.3×10^4 and NCCN is 0.23 - 0.24. The simulation of these parameters and maintaining the geometrical similarity of the nozzles made it impossible to maintain the diameter ratio between the jets and the wall of the combustion chamber same for the cold tests. For the development of the CFD code for prediction of the near nozzle flow this geometrical similarity is not essential. The relevant diameters of the prototype are listed in Table 1. The length of the primary annular duct of the prototype was 250 mm and the length of the secondary duct was 200 mm.

Table 1. Dimensions of the Prototype burner (multiply by 2 for the model in air; divide by 2 for model in water).

Quantities	Primary nozzle	Primary duct	Secondary nozzle	Secondary duct
Inner diameter	42 mm	42 mm	70 mm	70 mm
Outer diameter	50 mm	58 mm	78 mm	88 mm

Both the annular nozzles had the same annular gap (t) and the nominal velocity ratio (v_r) between the primary jet and the secondary jet was unity in most of the test cases discussed in this report. Therefore, further references to Reynolds number, in this document, is the number (Re_t) based on the average jet velocity and the annular opening of the nozzles at exit.

The experiments can be divided into four groups listed below, according to the flow field and the type of investigation conducted.

1. Prototype flow field investigation.
2. Axisymmetric stationary flow field investigation.
3. Instantaneous flow field investigation.
4. Numerical simulation of the flow fields.

The investigation of the prototype flow field and the axisymmetric stationary flow field were carried out in an air tunnel. The instantaneous flow fields were investigated in a water tunnel to overcome the limitations imposed by the digital particle image velocimetry (DPIV) hardware. Various aspects of DPIV are described in Raffel et al. (1998). All the computations reported here were limited to the flow field in water.

A gear compressor equipped with a frequency controller to drive it at a desired speed provides the air supply to the air tunnel. The horizontal cold chamber is constructed with a 386 mm inside diameter and 1200 mm long PVC tube. At the inlet, a section of the cylindrical wall measuring 400 mm along the circumference and 270 mm

axially was removed and a 0.08 mm thick transparent window was installed to gain optical access. In this setup a commercial smoke generator was used for flow visualization and incense smoke was used to seed the flow for LDV measurement. Descriptions of the model and test rig are given in Schmitt et al. (2001).

The water tunnel was constructed with its test section and settling chamber axis in the vertical direction. It was done to ensure that the coaxial position of the model is maintained with minimum of supports that are exposed to flow. The flow control through the burner model is achieved by keeping a high head across flow control nozzles. The flow control nozzles of different diameters determined the flow through the burner. Air filled glass spheres with mean diameter 9 μm and the specific gravity 1.02 was used for seeding.

The models to investigate the stationary and the instantaneous flow fields were designed to achieve axisymmetry in the exit streams. The flow passages in model for air was 2 times in size and the model for water was 0.5 times in size of the prototype. The two models were identical in length to diameter ratios of all the flow passages within 1% tolerance. The photographs of the smooth intakes and the nozzle exit face are shown in Figs. 4 and 5. The length to width ratio of the flow passages leading to the nozzles in all cases exceeded 40 to ensure fully

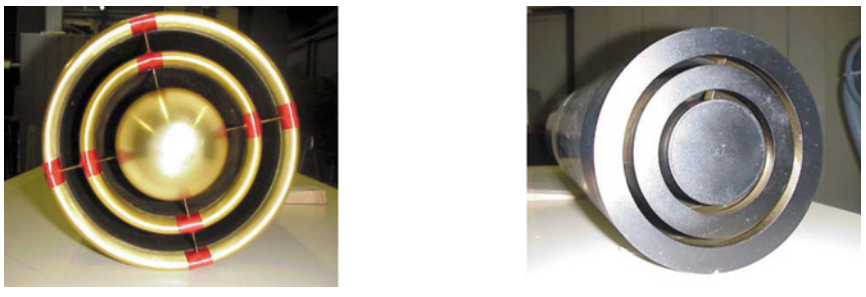

Fig. 4. The inlet and the exit of the model for air tunnel; diameters are two times those given in Table 1.

Fig. 5. The inlet and the exit of the model for water tunnel. The dimensions are shown in Fig. 6, the diameters are half of those given in Table 1.

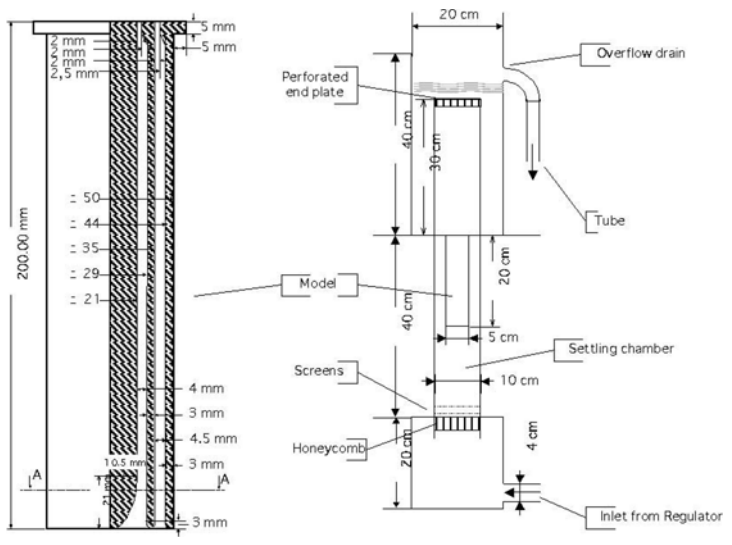

Fig. 6. Schematic diagrams of the model and test-rig used in DPIV.

developed turbulent profile. The total length of the equivalent prototype would have been 400 mm. In addition, starting from the settling chamber exit to the exit of the cold chamber all the components were arranged coaxially. Schematic diagrams of the model and the test rig used for DPIV are given in Fig. 6.

3.1 Experimens in the Model of the Prototype

The model of the burner was built with plastic tubes glued to the aluminum rings forming the double annular nozzles at one end and plastic discs at the other end. It was inserted in the horizontal cold chamber coaxially, face flush with the inlet plane wall of the chamber. The intake tubes of the burner model received metered amount of air or air-smoke mixtures from the compressor through flexible tubes. In this set-up, investigations were conducted by varying the velocity ratio of the secondary to primary streams as well as the Reynolds number.

The preliminary experiments were conducted in air with the prototype as well as a model twice the size of the prototype. The following investigations were conducted at various velocity ratios and Reynolds numbers in the cold test facility.

- LSV with video recording.
- Pressure survey along the centerline and the wall.
- LDV survey.

The mean thickness of the LSV laser sheet was 3 mm and the probe volume of the LDV was a cylinder of 0.1-mm diameter and 1-mm long.

The pressure survey and the LDV survey were conducted at secondary to primary velocity ratio range from 0.5 to 2 and Re_t range from 1300 to 4300.

3.2 Measurement of Stationary Flow Field in Axisymmetric Model

The model of the burner redesigned to deliver axisymmetric flow was built with plastic tubes glued to the aluminum rings forming the double annular nozzles at one end and the rings forming the smooth inlet at the other end. In this setup the cold chamber, model, the plenum chamber, the diffuser and the settling chamber were arranged coaxially in the horizontal position. The air from the compressor enters the settling chamber, flows through two screens and enters the diffuser containing 2 more screens. The air enters the plenum chamber where the intake of the burner is inserted. The exit end of the burner is inserted in the cold chamber with the face flush with the inlet end wall (see Schmitt et al., 2001).

The 2D LDV survey is conducted in this flow field in the meridional plane on a high-resolution grid. In the critical regions, the grid had spacing of the order of 5% of the nozzle opening. The survey was conducted at a nominal velocity ratio of 1 and at the Re_t of 3000. The probe volume was 0.1 mm in diameter and 1 mm long. The mean velocity and Reynolds stresses were derived from these measurements.

3.3 Measurement of Instantaneous Flow Field in Axisymmetric Model

These experiments were conducted in a water tunnel as mentioned before. The water from the flow regulator entered the settling chamber at the bottom of the test stand. The water then flowed through a honeycomb sandwiched between two screens and entered the plenum chamber. The burner model made from brass had 50-mm outer diameter and was 200 mm long. It was inserted from the top of the 95-mm diameter 400-mm long plenum chamber. The model extended to the middle of the plenum chamber. The 91-mm diameter 290-mm long cold chamber, where the burner delivered the water, was made with a 0.08-mm thick transparent sheet. The cold chamber was immersed in a 200-mm square cross-section tank from which water flowed out to a sump. Circulation was maintained by pumping the water back to the flow regulator tank.

The measurement and visualization techniques used in this test setup are,

- LSV in meridional and axial planes with CCD camera recording.
- DPIV in meridional plane.

The mean thickness of the light sheet used for LSV and DPIV was 2 mm. The LSV was conducted in the meridional and the axial planes at values of Re_t ranging from 10 to 3000 at a nominal velocity ratio of unity. DPIV investigations in the near nozzle region were conducted only in the meridional plane, under the same conditions in the range of Re_t from 40 to 2000. Detailed description and results of this experiment are published in Hazarika et al. (2001).

The DPIV system had a high-resolution (1026 × 1296 pixels) CCD camera and frame grabber for recording the images. A 4-watts Argon-ion laser was used as the power source. The pulses were generated with a Bragg cell driven by a RF generator. The RF generator was controlled with TTL signals coming from a synchronizer. The RF

generator could also be controlled from a signal generator. Therefore, it also resulted in a flexible system suitable for LSV study. The CCD camera is capable of recording 12 frames/second and the frame transfer time is 20 ms. This limited the time interval between two vector fields to 0.166 second. For flow visualization each frame was exposed for 83 ms; however, using the synchronizer, single short exposure frames were also taken. For multiple exposure in single frame a signal generator was used.

3.4 Numerical Simulations

Two different CFD codes were used for computations on 2D and 3D grids. All the computations were conducted for the model in water. Both codes included Navier-Stokes (N-S) solvers capable of calculating both laminar and turbulent flows. Several turbulence models such as algebraic Baldwin-Lomax (ABL) and variations of k-ε models (KEM) were implemented in these codes.

The first code, EURANUS, was a structured non-staggered grid code that solves the time-dependent 3D Reynolds averaged N-S (RANS) code. Multi-block approach was adopted to handle complex geometrical configuration (Hirsch and Khodak, 1995). Incompressible flows were simulated using preconditioning technique.

The second code, FlowVision, was based on modified finite volume approach where local refinement procedure was implemented making it an unstructured grid as a whole (Askenov et al., 1998). For the burner, RANS equation with k-ε turbulence model was solved to obtain the flow field.

All the computations were conducted for the model in water. For axisymmetric flow a 2-degree wedge shaped segment of the geometry was used for computation. In the EURANUS code the inlet ducts and the nozzles were included in the geometry. In the two inlet ducts, contractions and nozzles $129 \times 33 \times 2$ grids were used. In the cold chamber $257 \times 177 \times 2$ grids were used. The computations were completed for the laminar flow at $Re_t = 60$ and for turbulent flow using ABL at $Re_t = 2000$.

The computations with FlowVision were conducted in the cylindrical combustion chamber geometry. It gives a time accurate solution starting with an impulse flow at the inlet in time $t = 0$. The 2-degree wedge shaped geometry was used for the laminar and turbulent axisymmetric cases. A uniform grid of 100×250 with local adaptation at the inlet was used in the laminar calculations. For the turbulent calculations, uniform grids of 100×250 and 150×500 with local adaptations at the inlet were used. The computations were completed for the laminar flow at $Re_t = 60$ and for turbulent flow using KEM at $Re_t = 2000$.

The computation for the non-axisymmetric flow was conducted using FlowVision in the complete cylindrical cold chamber geometry. In this set of calculations $30 \times 30 \times 60$ grid with local adaptation at the inlet was used. The computation was completed for the laminar flow at $Re_t = 60$ with -3% and $+3\%$ asymmetry over diametrically opposite quarter sections of the inlet flow. Similar computations were also performed for -10% and $+10\%$.

All the measured and computed quantities are saved in the database described in Section 2, and the graphical presentations are produced using the tools mentioned there. The long sequence LSV images were made into a visualization movie. The sequences of vector fields obtained from DPIV were also inspected in animated form using the visualization tools.

4. Results and Discussion

All the experiments, conducted over a large range of flow conditions broadly exhibit the same topology of the mean flow field. In spite of the unsteadiness at low Reynolds number and the highly turbulent nature at higher range of Reynolds number the preliminary experimental results broadly defined the topology and the range of parameters for investigation. In all the experiments, both physical and numerical, the topology of the mean velocity field remained similar and is visible in all the figures shown in this section.

The near nozzle flow field is composed of three reverse flow regions separated by the jets. Starting near the axis and proceeding towards the wall they are,

1. A central toroidal vortex (CTV) enveloped by the primary jet at the burner face.
2. A pair of contra-rotating toroidal vortices (CVP) in the region between the burner face and the primary and the secondary jets.
3. An inside-out vortex (ORF) in the region between the secondary jet and the combustion chamber wall.

The calculations indicate the presence of the core flow along the axis of the cold chamber and counter flow along the wall. The topology of the near nozzle region was reproduced qualitatively for both laminar and turbulent flows. However, refinements of grids are required before validation of the codes could be carried out.

In the stationary test case the stagnation point is defined as the point on the axis where the combined jet meets and flow reverses. This point defines the extent of the central vortex. A circular stagnation curve is formed where the primary and the secondary jets meet and flow reversal occurs. This curve defines the extent of the contra-rotating vortex pair. Downstream of the stagnation point and upstream of the wall reattachment point, there are only two regions, the jet and the surrounding inside-out vortex. Flow visualization indicated reattachment, but computations did not predict it correctly.

The pressure survey at various velocity ratios between 0.5 and 2.0 and Reynolds number Re_t in the range between 1300 and 4300, showed that the pressure coefficient curve along the axis remains invariant with Re_t but changes with velocity ratio. This indicates that in this range of Re_t, the topology of the flow remains invariant as long as the velocity ratio remains fixed.

The LSV with video recordings showed the qualitative difference between the vortices. Amongst the large-scale structures, the time scale is smallest for the pair of contra-rotating vortices and largest for the inside-out vortex. The time scale is in the intermediate range for the central toroidal vortex.

The LDV measurements of the flow field of the prototype and its model in the air tunnel provided information regarding the deviation from axisymmetry. Surveys were conducted at 4 meridional planes 45 degrees apart. The non-axisymmetry was found to be highest in the meridional plane passing through the inlet tube axis and was close to +10% and −10% from the mean value. The flow visualization showed that the combined jet gradually moves away from the axis. The trend starts immediately downstream of the central vortex.

Figure 7 shows the turbulent flow in the axisymmetric model measured with LDV and the predicted flow field computed with EURANUS using ABL. In these figures selected number of mean velocity vectors (arrows) are plotted on the color background of its magnitude. Though the topologies revealed are quite similar, there are significant differences in the flow fields, these are discussed later in this section.

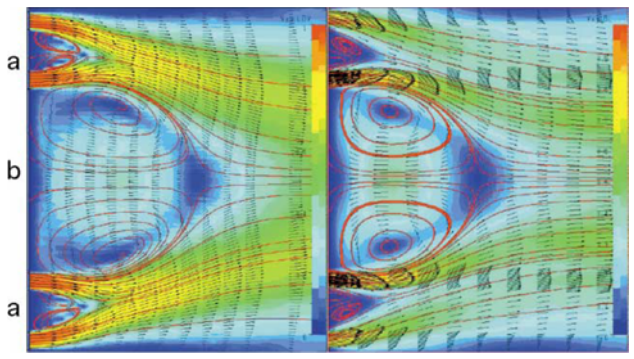

Fig. 7. Axisymmetric flow topology in meridional plane from LDV measurement (left, Re_t = 3000) and computation with EURANUS using ABL model (right, Re_t = 2000).

The LDV measurements showed high normal stress components in the near nozzle region. The highest value of the stress appears near the stagnation line between the primary and secondary jets. In the LSV at medium Reynolds number, rapid changes of the axial size of the pair of contra-rotating vortices are observed. The contribution by this oscillation is probably the cause of this high value. This region needs time series analysis of the velocity data. The continuous curves in both plots represent the particle-traces, which are identical to streamlines in the meridional plane for this case.

The LSV conducted at lower Re_t often showed unsteady flow structures. Figure 8 shows various situations encountered at Re_t = 60, the first image shows a nearly symmetric structure as measured with DPIV this shows all the regions described above. The second image obtained with LSV shows the break away of the central vortex. This manner of shedding of the central toroidal vortex is observed quite frequently at this Re_t. The third frame in this figure shows the particle-trace of laminar computation (FlowVision) results of axisymmetric (red), 3% asymmetry (black) and 10% asymmetry (blue) inlet flows. The particle-traces of the distorted inlet cases appear very similar to the flow when the vortex shedding occurs.

At higher Re_t another mechanism of vortex shedding was observed. The central toroidal vortex breaks up into several smaller structures before leaving this region. Figure 9 shows two images representing instantaneous flow fields and a mean flow field at Re_t = 180, the first image shows several distorted vortex structures in the

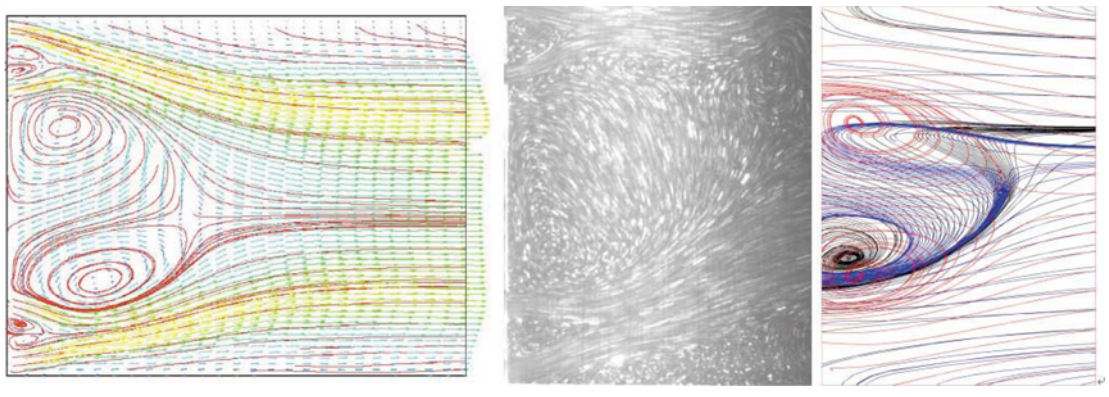

Fig. 8. Laminar flow at Re_t = 60: DPIV of nearly axisymmetric flow, LSV of vortex shedding and CFD at various degrees of non-axisymmetric flow.

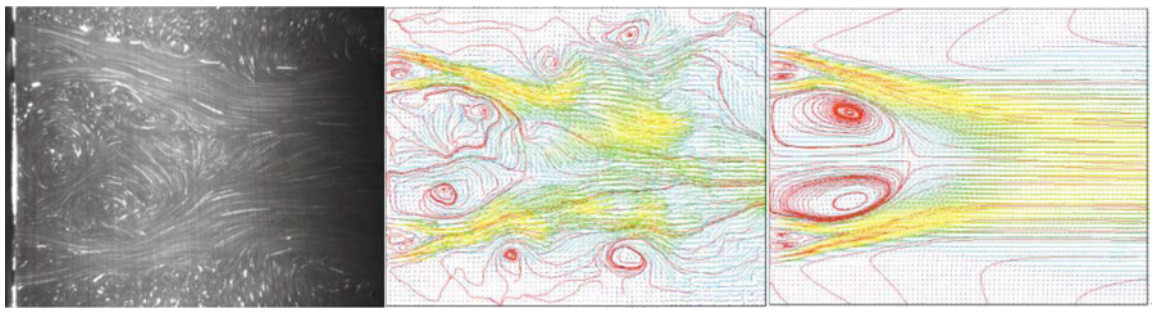

Fig. 9. Flow during transition of the flow field at Re_t = 180. From left to right, LSV image, instantaneous field from DPIV and mean of 250 vector fields from DPIV.

central region in the meridional plane. The second image shows a vector field obtained with DPIV and various structures highlighted using numerical particle traces. Several eddy structures, other than the mean vortices, are visible in the reverse flow regions. These eddy structures disappear in mean flow field obtained from these vector fields. With increasing Reynolds number these eddy structures multiply in numbers. This is believed to be the mechanism leading to turbulent flow. The structures could be identified in flow field obtained at Re_t = 2000. From this study it could be argued that the transition from laminar to turbulent vortex goes through the process of breakdown to multiple vortices.

In all the cases studied here (Re_t = 40 to 3000) the contra-rotating vortex pair did not show any vortex shedding. However, the extents of the region in the axial direction as well as the relative sizes of the vortex pair were observed to fluctuate all the time. At Re_t = 60 DPIV of a close-up of the vortex pair on one side was conducted. This sequence gives high-resolution vector fields in this region. An animation of the fluctuating vortex pair was created with the sequence to study this field.

The results of the laminar computation for axisymmetric inlet and the average of few selected axisymmetric field are plotted in a color-map and compared in Cartesian plot in Fig. 10. The Cartesian plots are made along the section of the contra-rotating vortex pair (short curves) and along the central toroidal vortex (long curves). The numbers in the color maps indicate velocity. These figures show that the sizes of the various regions were predicted longer than the measured regions. The trend is opposite of that in turbulent flow computation. The prediction of higher rate of velocity decay near the nozzle and longer length for merging of jets are the defects of this laminar computation also.

In spite of the deficiency of CFD in predicting complex flow fields correctly, it could provide valuable insight. A comparison of flow fields for laminar case with axisymmetric and asymmetric inlet conditions is shown in Fig. 8. The particle traces obtained from computation is a comparison of the particle-traces between the axisymmetric, 3% distorted and 10% distorted flows. The similarity of these particle-traces with the LSV image leads one to believe that the unsteadiness in the laminar flow could be a result of distortion of the flow at the exit of

the nozzles. More investigation is required in this direction to understand the precise nature of this phenomenon.

The results of the computations using KEM of Chien (1982) is shown in Fig. 11 along with the mean vector field found from the PIV measurements at the same flow conditions (Re_t = 2000). In these figures the vectors themselves are color coded for magnitude. Here also, the computed and the measured velocity fields show differences similar to those for Fig. 7. The prediction with KEM model was only marginally better than that by ABL model. The differences between the computed and measured topologies are (Figs. 7 and 11):

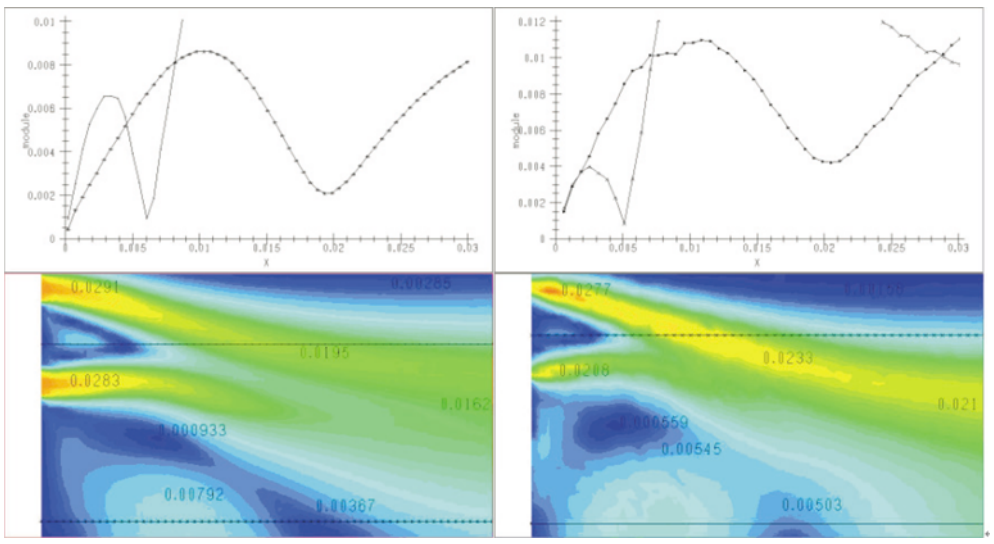

Fig. 10. Axisymmetric flow at Re_t = 60, computed (left) and measured (right).

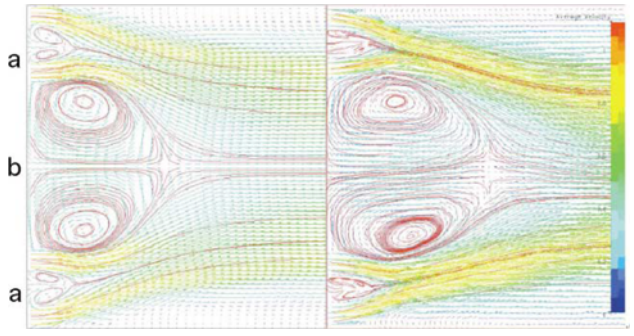

Fig. 11. Computed flow field using KEM of Chien (left) and flow field measured with DPIV (right) at Re_t = 2000.

1. The axial length of the central toroidal vortex was predicted 10% shorter (region indicated as "a" in the two figures).
2. The axial length of the pair of contra-rotating vortices was predicted 30% shorter (regions indicated as "b" in the two figures).
3. Comparatively rapid velocity decay of the jets closer to the exit of the nozzles was predicted.
4. Merging of the primary and the secondary jets were predicted at larger axial distance than it was found from LDV and DPIV measurements (compare color codes in Figs. 7 and 11).

The evolution of the near nozzle flow vector field was easily recorded by the DPIV system at lower Re_t. The system also recorded the evolution of the contra-rotating vortex pair between the two jets at the same Re_t. However, the time interval between two consecutive vector fields (0.166 s) is not close enough to capture the evolution of the coherent structures in the turbulent flows, even though they are identified in the velocity vector and vorticity contour plots. In case of the intermediate range of Re_t (100 to 500), it is possible to capture six vector fields in a second, which is adequate for the study of the largest vortex structures. The presence of the large coherent structures in the instantaneous vector field and the similarity of these structures to those seen at the

intermediate range of Re_t suggest that the transition of the flow-field from laminar to turbulent occurs gradually. A more systematic study combining time series analysis of hot-wire signals, DPIV and large eddy simulation (LES) will lead to more realistic picture of the flow.

5. Conclusions

The study of complex flows using integrated EFD and CFD approach improves the understanding of such flow field, as shown in the burner test case presented here. During the process, the flow visualization tools were essential to examine the flow physics and compare the results.

It was found that the commercial CFD codes RANS solvers with ABL or KEM for turbulence are not suitable to predict the flow in a bluff body flame holder. The experimental investigation of the flow should be combined with LES to gather more information in order to develop realistic turbulence models.

The QFView system under development will solve the important aspect of the new generation of visualization tools, which need to be fully integrated with the large fluid flow databases. Such functionality could reduce the experiments cost and design by reusing the reliable and validated fluid dynamics computations and experiments.

Acknowledgments

The authors gratefully acknowledge the support of the ALICE consortium partners and the financial support provided by the EC DG-XIII via the ESPRIT-IV ALICE project (EP-28168) during this work.

The authors wish to acknowledge the contribution by Dr. S. Zhuktov in conducting the computations using FlowVision, contributions by Dr. F. Schmitt in providing the LDV data and Mr. P. Brajak for the development of eMedia 2000.

References

Askenov, A., Dyadkin, A. and Pokhilko, V., Overcoming of Barrier between CAD and CFD by Modified Finite Volume Method, Proceedings of the ASME Pressure Vessels and Piping Division Conference, (1998).

BEA WebLogic E-Business Platform, http://www.bea.com, (2001).

Chien, K. Y., Predictions of Channel and Boundary Layer Flows with a Low Reynolds Number Turbulence Model, AIAA Journal, 20-1 (1982), 33-38.

EJB, Enterprise JavaBeans technology, http://java.sun.com/products/ejb, (2001).

Gharib, M., Perspective: the Experimentalist and the Problem of Turbulence in the Age of Supercomputers, Journal of Fluids Engineering, 118-2, (1996), 233-242.

Guruz, A. G., Guruz, H. K., Osuwan, S. and Steward, F. R., Aerodynamics of a Confined Burning Jet, Combustion Science and Technology, 9 (1974), 103-110.

Hazarika, B. K., Vucinic, D., Schmitt, F. and Hirsch, C., Analysis of Toroidal Vortex Unsteadiness and Turbulence in a Confined Double Annular Jet, AIAA 39th Aerospace Sciences Meeting and Exhibit, (2001), AIAA 2001-0146.

Hirsch, C. and Khodak, A. E., Modeling of Complex Internal Flows with Reynolds Stress Algebraic Equation Model, 26th AIAA Fluid Dynamics Conference, (1995), AIAA 95-2246.

J2EE, Java 2 Platform, Enterprise Edition, http://www.javasoft.com/j2ee, (2001).

JSP, Professional Java Server Programming, J2EE Edition, Oct., (2000), Wrox Publishing.

Raffel, M., Willert, C. and Kompenhans, J., Particle Image Velocimetry : A Practical Guide, (1998), Springer-Verlag, Berlin Heidelberg.

RDBMS, Informix Dynamic Server 2000 database server, http://www.informix.com/ids2000, (2001).

Schmitt, F., Hazarika, B. K. and Hirsch, C., LDV Measurements of the Flow Field in the Nozzle Region of a Confined Double Annular Burner, Journal of Fluids Engineering, 123-2 (2001).

Steward, F. R. and Guruz, A. G., Aerodynamics of a Confined Jet with Variable Density, Combustion Science and Technology, 16 (1977), 29-45.

Vucinic, D., Barone, M. R., Sünder, B., Hazarika, B. K. and Tanzini, G., QFView - An Internet Based Archiving and Visualization System, AIAA 39th Aerospace Sciences Meeting and Exhibit, (2001), AIAA 2001-0917.

Vucinic, D., Favaro, J., Sünder, B., Jenkinson, I., Tanzini, G., Hazarika, B. K., Ribera d'Alcala, M., Vicinanza, D., Greco, R. and Pasanisi, A., Fast and Convenient Access to Fluid Dynamics Data via the World Wide Web, European Congress on Computational Methods in Applied Sciences and Engineering ECCOMAS 2000, (2000).

Vucinic, D., Pottie, M., Sotiaux, V. and Hirsch, C., CFView - An Advanced Interactive Visualization System Based on Object-oriented Approach, AIAA 30th Aerospace Sciences Meeting and Exhibit, (1992), AIAA 92-0072.

Author Profile

Dean Vucinic: He received his Dipl.-Ing. degree in Shipbuilding in 1982 from Technical Faculty, University of Rijeka. He worked in the shipyard 3MAY Rijeka as a Naval Architect and CAD/CAM expert. From the same university in 1987 he received the M.Sc. degree in Technical Sciences.In 1988 he joined the Department of Fluid Mechanics, Vrije Universiteit Brussel, where he developed "CFView - Computational Field Visualization System", interactive visualization software adapted to the graphics requirements of numerical simulation tools. His research interest in Scientific Visualization for Computational and Experimental Fluid Dynamics (Ph.D. thesis in progress), involves object-oriented software design, interactive computer graphics and web based multimedia tools for multidisciplinary research in engineering.
He is currently involved in two European RTD projects. He is a project manager of the ESPRIT-FP4 project ALICE and coordinating GROWTH-FP5 project QNET-CFD.

Birinchi Kumar Hazarika: He received his B.E. degree in Mechanical Engineering in 1973 from Birla Institute of Technology and Science, Pilani, India, M.E. degree in Mechanical Engineering in 1975 from Indian Institute of Science, Bangalore, India and Ph.D. in 1987 from The City University of New York, New York, USA. During the period between master's and doctoral degree, he worked as Assistant Lecturer at B. I. T. S., Pilani, India, Scientist at Gas Turbine Research Establishment, Bangalore, India and Adjunct Lecturer at The City College of CUNY, New York, USA. After the Ph.D. he worked as Research Associate at Vrije Universiteit Brussel, Belgium and as Visiting Assistant Professor at Indian Institute of Technology, Kanpur, India. He is currently working as Research Associate at Vrije Universiteit Brussel in the area of Experimental Fluid Dynamics.